

This supplementary information was **updated** on **19<sup>th</sup> June 2020**.

### **Tunneling-current-induced local excitonic luminescence in p-doped WSe<sub>2</sub> monolayers**

This supplementary information has been updated to reflect the following changes:

- The caption of Figure S1 previously mentioned the absence of a “ $G_{2g}^1$ ” interlayer Raman mode around 300 cm<sup>-1</sup>. This has been corrected to “ $B_{2g}^1$ ”.
- The colour of the yellow curve in Figure S9(c) was changed for better visibility.

Please contact [Nanoscale@rsc.org](mailto:Nanoscale@rsc.org) with any inquiries, citing the DOI: [doi.org/10.1039/D0NR03400B](https://doi.org/10.1039/D0NR03400B)

# Electronic Supplementary Information

## Tunneling-current-induced local excitonic luminescence in p-doped WSe<sub>2</sub> monolayers

Ricardo Javier Peña Román,<sup>\*a</sup> Yves Auad,<sup>a</sup> Lucas Grasso,<sup>a</sup> Fernando Alvarez,<sup>a</sup> Ingrid David Barcelos<sup>b</sup> and Luiz Fernando Zagonel<sup>\*\*a</sup>

Figure S1: Pre-characterization of WSe<sub>2</sub> samples

Figure S2: AFM profiles before and after thermal annealing

Figure S3: Localization of exfoliated monolayer WSe<sub>2</sub> inside STM

Figure S4: STM images in UHV conditions and densities of point defects in monolayer WSe<sub>2</sub>

Figure S5: STM-LE quantum yield and temporal stability of the STM-LE signal

Figure S6: Excitonic STM-LE spectra with different tunneling parameters

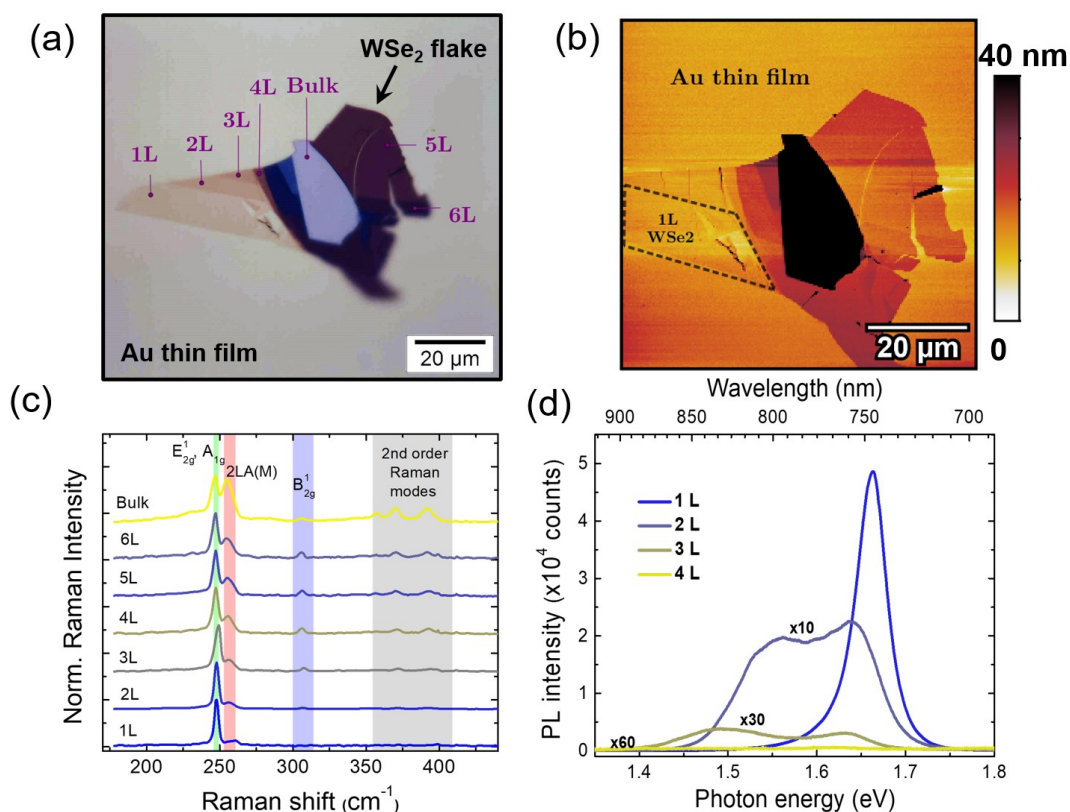
Figure S7: Neutral exciton and trion emissions in STM-LE and PL spectra

Figure S8: Trion and neutral exciton emission ratio

Figure S9: Exciton and plasmon emission with different tunneling parameters

\* [rikrdopr@ifi.unicamp.br](mailto:rikrdopr@ifi.unicamp.br)

\*\* [zagonel@ifi.unicamp.br](mailto:zagonel@ifi.unicamp.br)



**Figure S1:** Pre-characterization of an exfoliated WSe<sub>2</sub> flake transferred to 100 nm Au thin film on Si substrate. (a) Optical microscopy image. The optical contrast in the gold substrate helps to identify regions with a different number of layers. (b) Atomic Force Microscopy (AFM) image showing regions with different heights and imperfections created in the flake during the transferring process. (c) Raman and (d) photoluminescence spectra at room temperature. The monolayer WSe<sub>2</sub> has been confirmed by the absence of the interlayer Raman mode ( $B_{2g}^1$ ) around 300 cm<sup>-1</sup>, as well as, by the strong PL peak at 1.65 eV. The Raman and PL spectra have the same characteristic of those observed in samples deposited on silicon dioxide substrates<sup>1-4</sup>, indicating that in as-transferred samples there is no coupling between the TMD and the metallic substrate (quenching effects are not observed).

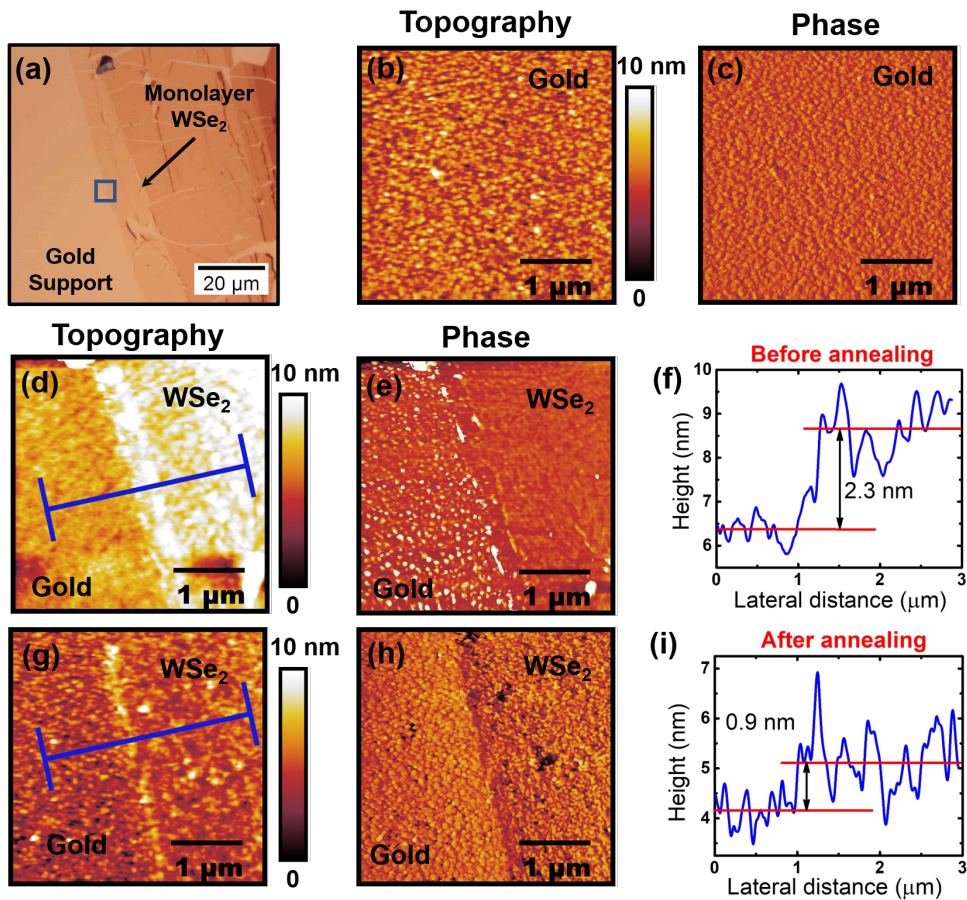


**Figure S2:** (a) Optical microscope image showing the Monolayer WSe<sub>2</sub> on top of the gold substrate. (b) Topography and (c) Phase AFM images of the gold substrate. (d) Topography and (e) Phase AFM images of the interface between the gold substrate and the monolayer WSe<sub>2</sub> before the 400 K thermal annealing in UHV for 12 hours. (f) AFM line profile obtained from (d) averaging a 3 μm long and 1 μm large area indicating a step height of 2.3 nm. (g) Topography and (h) Phase AFM images of the interface between the gold substrate and the monolayer WSe<sub>2</sub> after the 400 K thermal annealing in UHV for 12 hours. (i) The AFM line profile obtained from (g), averaging a 3 microns long and 1 μm large area, indicates ~0.9 nm of step height. Since the expected thickness of the monolayer WSe<sub>2</sub> is about 1 nm, we consider that before the thermal annealing in UHV there was a water layer under the TMD.

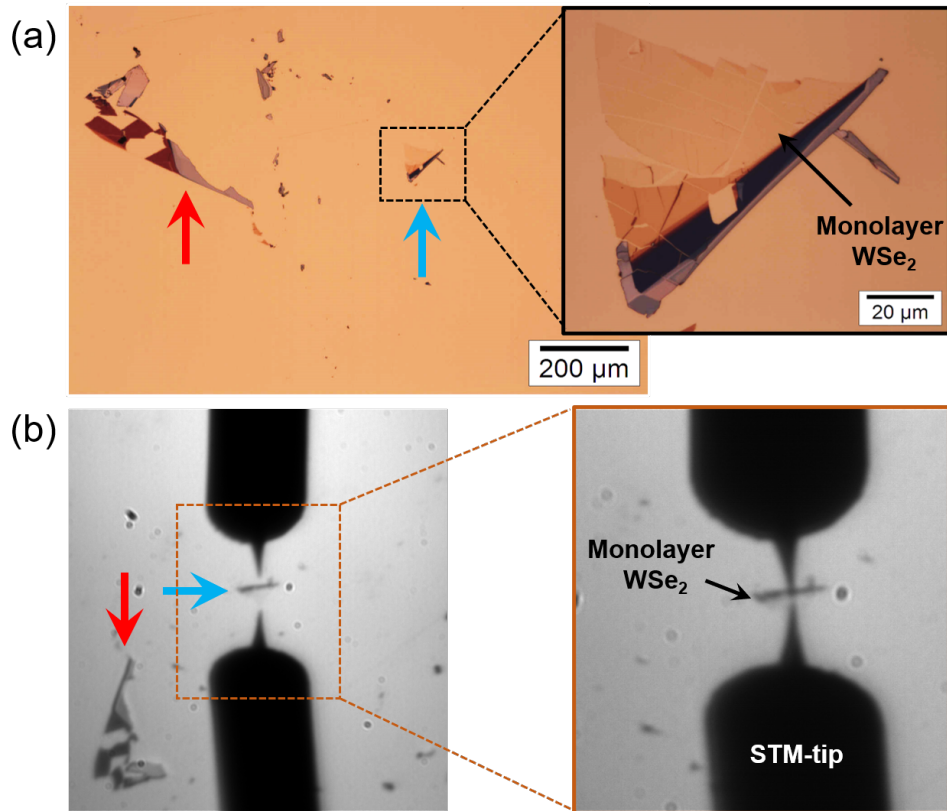


**Figure S3:** Localization of the flake of interest inside the STM microscope for the tip approach. (a) Optical microscopy image. The flake indicated by the red arrow is used as a reference point to localize the flake of interest with monolayer WSe<sub>2</sub> as indicated by the blue arrow. (b) By using a zoom lens, the monolayer WSe<sub>2</sub> is localized inside the STM, and the tip is approached. In the image, the STM tip and its reflection on the metallic substrate are observed. The tip wire diameter is 250 μm. This procedure is the same for STM measurements in UHV, and STM-LE in air.

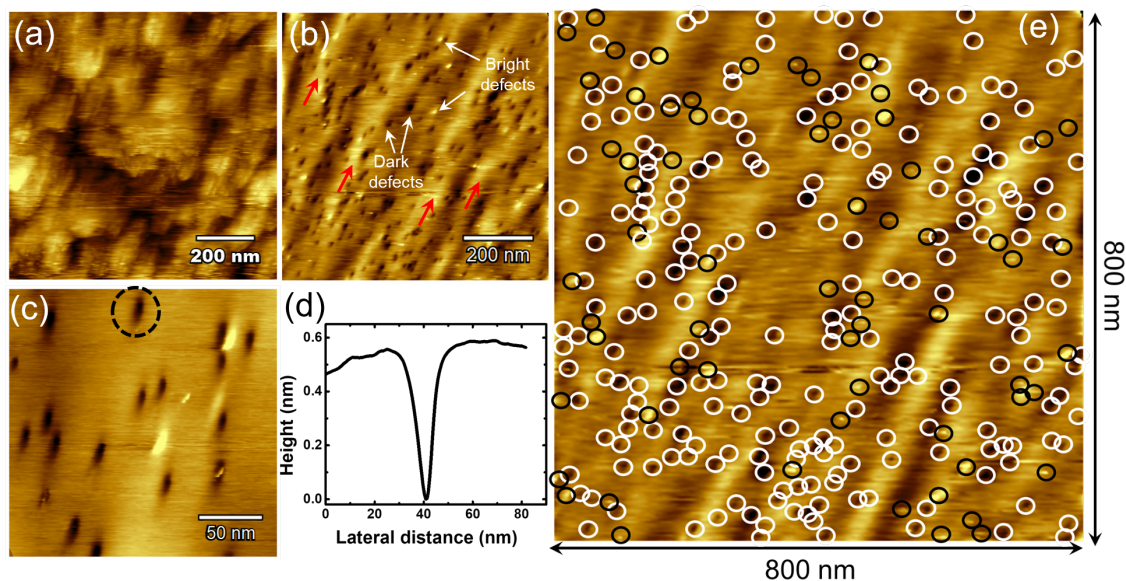


**Figure S4:** STM images obtained in UHV at room temperature in monolayer  $\text{WSe}_2/\text{Au}/\text{Si}$  annealed at 400 K. (a) STM-image of  $1.0 \mu\text{m} \times 1.0 \mu\text{m}$  of the Au thin film surface (3.5 V, 300 pA). (b) STM-image of  $0.8 \mu\text{m} \times 0.8 \mu\text{m}$  of the  $\text{WSe}_2$  surface (1.0 V, 65 pA). A surface height undulation (red arrows) is observed in addition to some dark and bright point defects. (c) STM-image of  $226 \text{ nm} \times 226 \text{ nm}$  of the  $\text{WSe}_2$  surface (1.0 V, 65 pA) showing dark defects and (d) the depth profile of one of them. (e) Quantification of the defects density in the image shown in (b). Dark and bright defects are indicated in white and black circles, respectively.

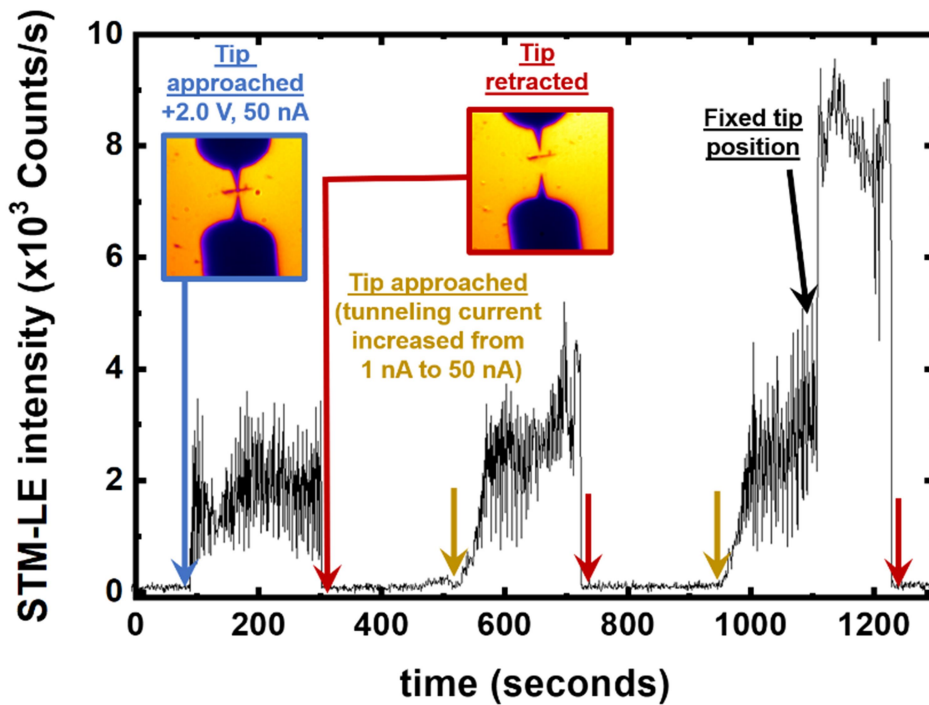


**Figure S5:** The STM-LE signal was recorded panchromatically as a function of time using a PMT to evaluate the quantum yield and temporal stability. Three cycles of tip approach and retraction are shown. Sample bias is set to 2.0V, and the tunneling current increased up to 50 nA. The results indicate the variation of the observed signal as well as the ease of getting the signal back after establishing a tunneling current. The signal variations are also observed due to the short PMT integration time: 0.3 seconds. Similar variations are typically observed in the tunnel current, as one could expect in air<sup>5</sup>. In the first 1100 s (~18 minutes) the signal was acquired scanning the tip on a surface area of 130 nm × 130 nm, after that the STM tip position was fixed, and signal of about  $9 \times 10^3$  counts per second was obtained with 50 nA. This gives a Quantum Yield (QY) of  $\sim 5 \times 10^{-7}$  photons per electron, similar to observed in MoSe<sub>2</sub> mechanically transferred on ITO<sup>6</sup>.

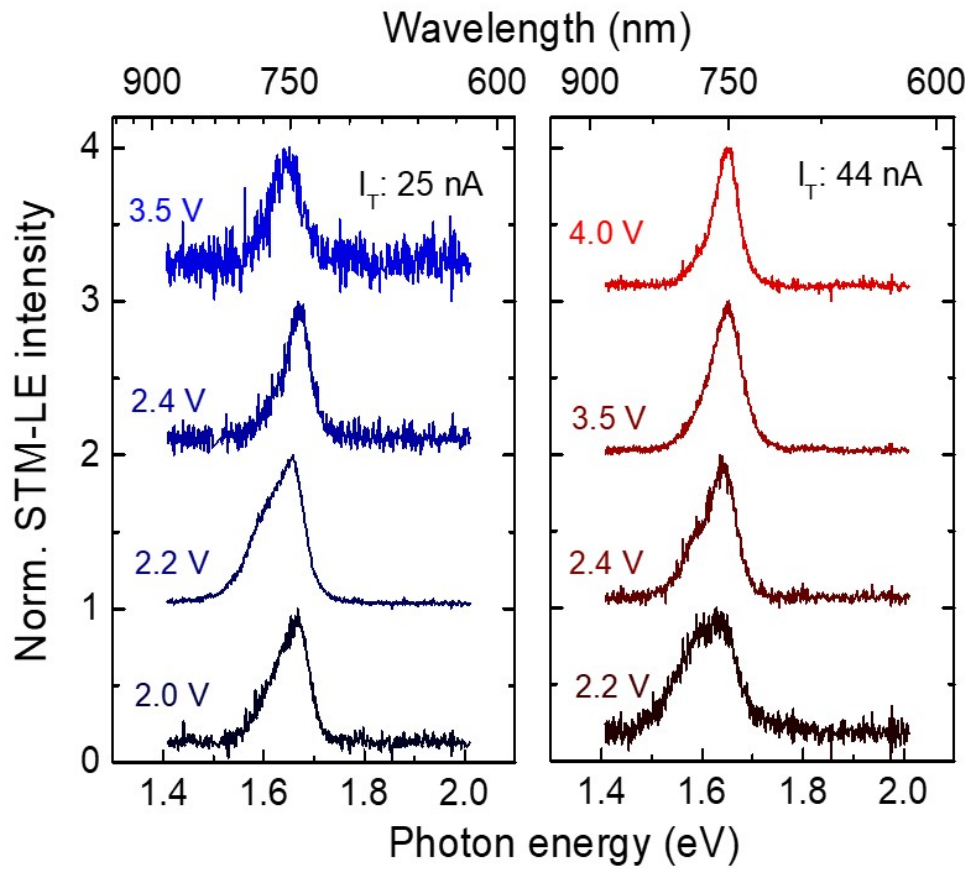


**Figure S6:** STM-LE spectra measured with different sample bias and tunneling currents of 25 nA (black to blue curves) and 44 nA (black to red curves), the integration time per spectrum was of 100 s. Some different peak shapes are observed due to the different intensities of the charged exciton (trion) and of the neutral excitons. See the decomposed spectra in Figure S7 and the ratio as a function of sample bias in Figure 3(c). The center of each emission remains roughly at the same energy, as shown in Figure S8. That is, no systematic energy shift is observed in the STM-LE peak as a function of the sample bias. The same spectral features are observed both at 25 nA and at 44 nA.

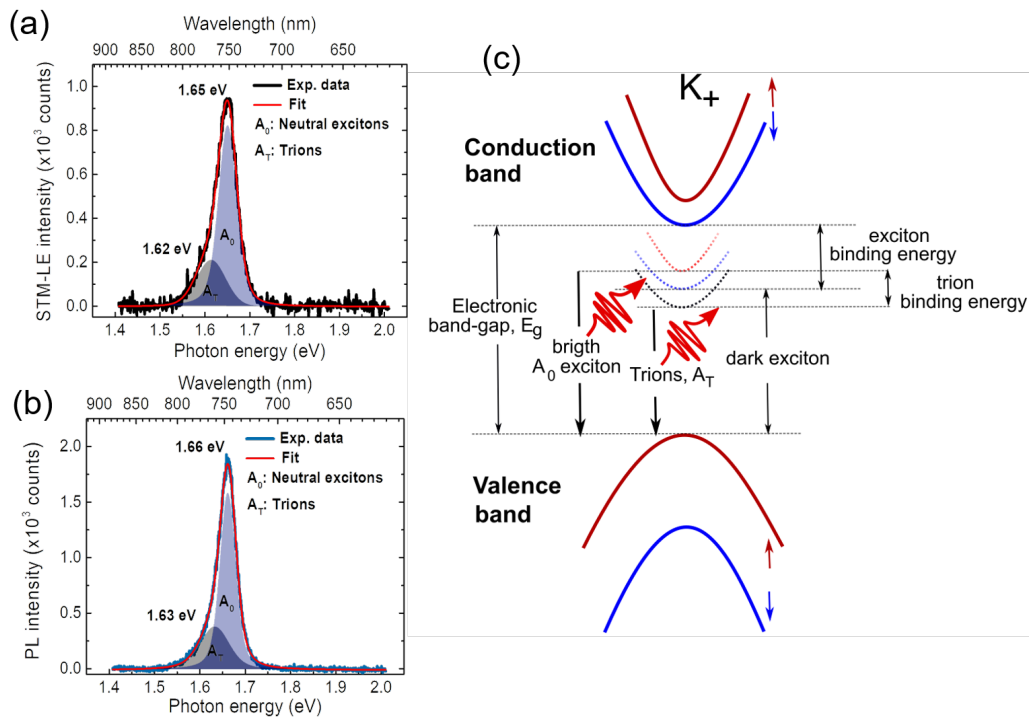


**Figure S7:** (a) STM-LE (4.0 V, 44 nA) and (b) PL spectra of monolayer WSe<sub>2</sub> fitted with two Voigt peaks associated with the emission due to bright A neutral excitons (A<sub>0</sub>) recombination and trions (A<sub>T</sub>) recombination. (c) The schematic diagram for the energy levels in monolayer WSe<sub>2</sub> at the K<sub>+</sub> point of the Brillouin zone showing the direct electronic band-gap, binding energy for excitons and trions, and the recombination A<sub>0</sub> and A<sub>T</sub>. According to reference <sup>7</sup>, the electronic band gap is 2.0 eV, and the exciton binding energy is 0.37 eV. Hence, the neutral exciton emission from single-layer WSe<sub>2</sub> is expected at 1.65 eV, as observed here.

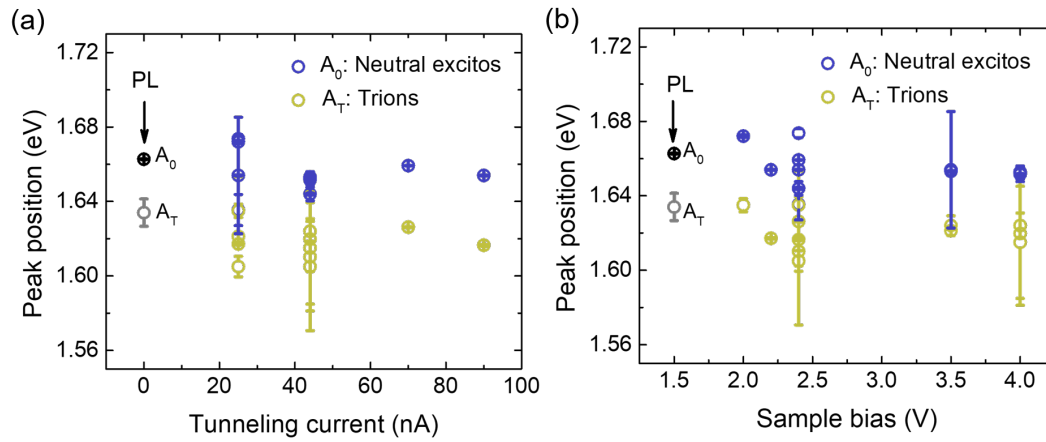


**Figure S8:** Position of the charged exciton (trion) and neutral exciton obtained from decomposing of STM-LE spectra. The spectra considered included those in Figure 2(c), 3(a), S6, and S7. In these cases, no plasmon contribution is observed, and all spectra can be decomposed as (and adjusted with) 2 peaks related to trion and neutral exciton emission. In (a) the position of the peaks is shown as a function of the tunneling current and in (b) as a function of the sample bias. In both cases, no systematic shift is observed. The small energy variation shown in these graphs is possibly related to the difference between each region on the monolayer  $\text{WSe}_2$  that can be subjected to different stress states or have slightly different defect concentration. In (a) and in (b), the energy of both trion and neutral exciton obtained from low power PL (spectrum in Figure S7) is indicated for comparison. For the PL acquisition, there was no tunneling current or sample bias voltage.

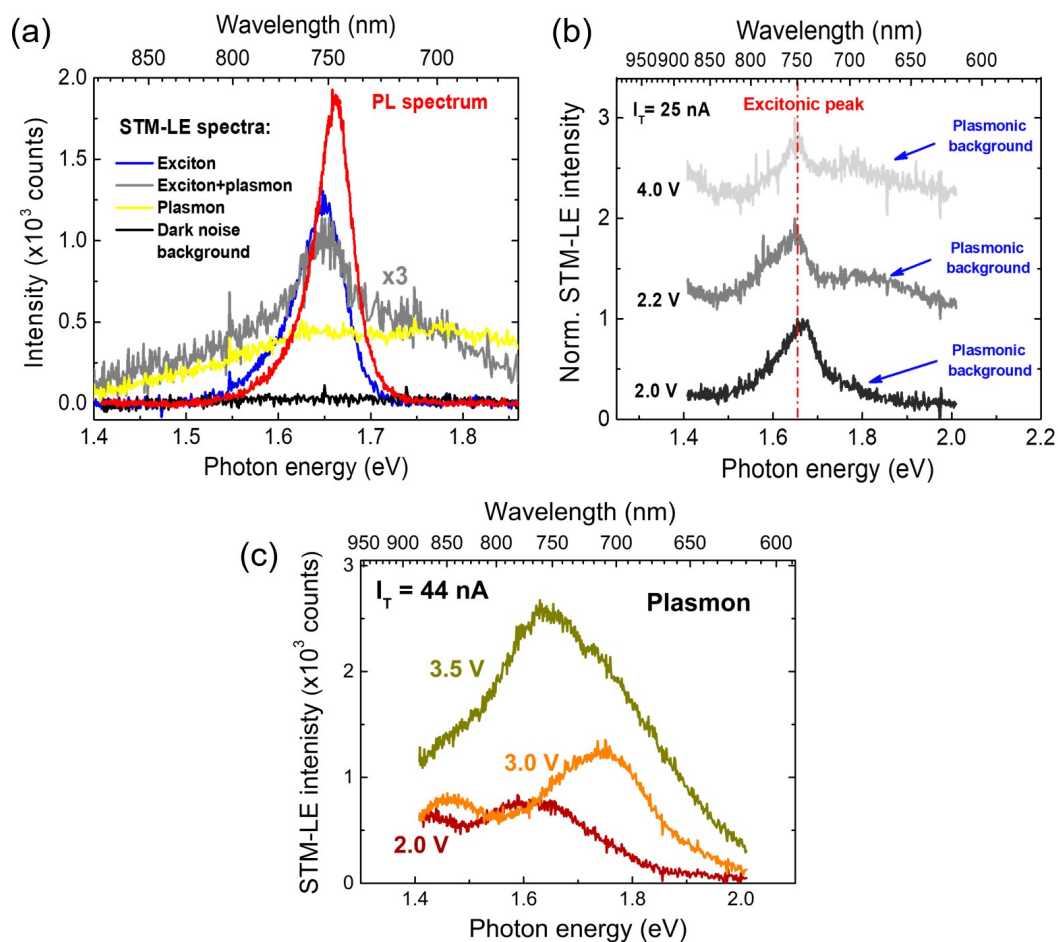


**Figure S9:** In (a), for comparison, the raw data of different spectra are shown, including the CCD dark noise, one PL spectrum, one STM-LE excitonic spectrum, one STM-LE with both plasmonic and excitonic emission and one STM-LE purely plasmonic. The STM-LE excitonic spectrum closely resembles the PL spectrum. In contrast, spectra with plasmonic contributions are readily spotted as much broader spectrally, covering the whole spectral range (as observed comparing them with the dark noise background). (b) STM-LE spectra of the simultaneous excitonic and plasmonic emission obtained with different tunneling parameters. (c) Pure plasmonic emission due to the gold metallic support for different sample bias voltage. The spectra obtained in (b) and (c) were recorded in the same sample region where high sample bias and high tunneling current was applied or in the same region where ‘tip pulse’ procedures were performed. A ‘tip pulse’ is a procedure in which the tip is put in contact with the sample (short circuit) for a brief moment to induce tip reconstruction.

## References

1. Tonndorf, P. *et al.* Photoluminescence emission and Raman response of monolayer MoS<sub>2</sub>, MoSe<sub>2</sub>, and WSe<sub>2</sub>. *Opt. Express* **21**, 4908 (2013).
2. Zeng, H. *et al.* Optical signature of symmetry variations and spin-valley coupling in atomically thin tungsten dichalcogenides. *Sci. Rep.* **3**, 4908–4916 (2013).
3. Terrones, H. *et al.* New First Order Raman-active Modes in Few Layered Transition Metal Dichalcogenides. *Sci. Rep.* **4**, 1–9 (2014).
4. Zhao, W. *et al.* Lattice dynamics in mono- and few-layer sheets of WS<sub>2</sub> and WSe<sub>2</sub>. *Nanoscale* **5**, 9677 (2013).
5. Rogez, B. *et al.* The mechanism of light emission from a scanning tunnelling microscope operating in air. *Nanotechnology* **27**, (2016).
6. Pommier, D. *et al.* Scanning Tunneling Microscope-Induced Excitonic Luminescence of a Two-Dimensional Semiconductor. *Phys. Rev. Lett.* **123**, 1–7 (2019).
7. He, K. *et al.* Tightly bound excitons in monolayer WSe<sub>2</sub>. *Phys. Rev. Lett.* **113**, 1–5 (2014).